A New Method for Accurate and Efficient Modeling of the Local Ocean Induction Effects. Application to Long-Period Responses from Island Geomagnetic Observatories

Chaojian Chen[1], **Mikhail Kruglyakov**[1,2], **Alexey Kuvshinov**[1]

[1]Institute of Geophysics, ETH Zurich, Switzerland
[2]Geoelectromagnetic Research Center, Institute of Physics of the Earth, Moscow, Russia

Key Points:

- A global-to-Cartesian (G2C) EM modeling tool was developed to account for effects in long-period responses from local bathymetry
- Model studies using the G2C tool show that local bathymetry dramatically influences responses at island geomagnetic observatories
- G2C makes it possible to explain anomalous behavior of the observed responses at island observatories

Corresponding author: Chaojian Chen, `chaojian.chen@erdw.ethz.ch`

Abstract

There is significant interest in constraining mantle conductivity beneath oceans. One data source to probe oceanic mantle conductivity is magnetic fields measured at island observatories. From these data local responses are estimated and then inverted in terms of conductivity. However, island responses may be strongly distorted by the ocean induction effect (OIE) originating from conductivity contrasts between ocean and land. Insufficiently accurate accounting for OIE may lead to wrong interpretation of the responses. OIE is generally modeled by global simulations using relatively coarse grids to represent bathymetry. We explore whether very local bathymetry influences island responses. To address this question we developed a methodology for efficient modeling of effects of bathymetry of any resolution. On an example of two island observatories we demonstrate that small-scale bathymetry dramatically influences the responses. Using new methodology we obtain new conductivity models beneath considered islands and observe remarkable agreement between modeled and experimental responses.

1 Introduction

Determining the three-dimensional (3-D) distribution of physical properties in Earth's mantle attracts widespread interest in the geosciences. Seismic tomography provides a variety of global 3-D velocity models, but the interpretation of seismic velocities in terms of thermodynamics is often uncertain, especially when it comes to constraints on water content [*Fei et al.*, 2017; *Schulze et al.*, 2018; *Buchen et al.*, 2018]. An alternative way to probe the Earth's mantle is by means of Geomagnetic Depth Sounding (GDS), which exploits magnetic field variations of magnetospheric and/or ionospheric origin to constrain the electrical conductivity at depth. From these data local GDS responses (cf. *Banks* [1969]) are estimated and then inverted in terms of conductivity. Since conductivity is sensitive to temperature, hydrogen content, and the presence of melt [*Yoshino*, 2010; *Karato*, 2011; *Karato and Wang*, 2013; *Yoshino and Katsura*, 2013; *Khan*, 2016], mapping this property constrains the chemistry and physical state of the mantle. GDS mostly relies on the data coming from a global network of geomagnetic observatories. However, bearing in mind the very irregular spatial distribution of the geomagnetic observatories (with substantial gaps in oceanic regions), the recovery of a cogent 3-D mantle conductivity model beneath oceans from observatory data is probably not feasible. At most one can decipher local one-dimensional (1-D) conductivity profiles beneath island observatories and explore lateral variability of the recovered 1-D mantle structures. The challenge here is that the GDS responses at island observatories may be strongly distorted by the effects from lateral conductivity contrast between land and ocean (the ocean induction effect; OIE) [*Parkinson and Jones*, 1979; *Kuvshinov et al.*, 2002], which in its turn may lead to misinterpretation of the results, if OIE is not accurately enough accounted or corrected for. Over the last decade, a number of GDS studies were carried out with the goal of constraining 1-D conductivity distributions beneath coastal and island geomagnetic observatories [*Khan et al.*, 2011; *Munch et al.*, 2018; *Guzavina et al.*, 2019]. The OIE was modeled in these papers using a global 3-D EM forward modeling code X3DG [*Kuvshinov*, 2008] which is based on an integral equation (IE) approach, and is benchmarked in a number of publications [*Yoshimura and Oshiman*, 2002; *Kelbert et al.*, 2014; *Velímský et al.*, 2018, among others]. Due to the high computational costs of global 3-D forward simulations, relatively coarse lateral grids (with at best $0.25° \times 0.25°$ resolution) were used to represent the OIE. However, the pronounced disagreement between modeled and observed (i.e. estimated from the data) GDS responses detected by *Munch et al.* [2018] at a number of island observatories raises the question of whether this discrepancy is due to very local bathymetry which is not accounted for in “coarse grid” modeling.

To address this question we developed a global-to-Cartesian (G2C) electromagnetic (EM) forward modeling methodology (described in Section 2) which also exploits the IE approach but allows us to efficiently calculate the EM responses in the problem setups requiring highly detailed bathymetry in the (local) region of interest. In Section 3 we compute long-period responses at two island (Cocos-Keeling and Honolulu) geomagnetic observatories by exploiting different – from rather coarse $1° \times 1°$ to very fine $0.01° \times 0.01°$ – lateral grids, and demonstrate that very local bathymetry variations substantially influence the GDS responses at periods as long as 20 days. By using the responses computed at $0.01° \times 0.01°$ grid, we obtain new 1-D conductivity models beneath considered islands and observe remarkable agreement between modeled and experimental responses. In particular, we reproduce the anomalous behavior of responses at Cocos-Keeling observatory. Finally, in Section 4 we summarize the findings of the paper, and discuss the potential ways to better constrain conductivity distribution in oceanic mantle.

2 Methods

2.1 Conventional IE approach

In the frequency domain and for a given 3-D conductivity model of the Earth, σ, and a given source, $\mathbf{j}^{ext}$, the electric, $\mathbf{E}$, and magnetic, $\mathbf{H}$, fields obey Maxwell's equations:

$$\nabla \times \mathbf{H}(\mathbf{r}) = \sigma(\mathbf{r})\mathbf{E}(\mathbf{r}) + \mathbf{j}^{ext}(\mathbf{r}), \quad (1)$$

$$\nabla \times \mathbf{E}(\mathbf{r}) = i\omega\mu_0\mathbf{H}(\mathbf{r}), \quad (2)$$

where $i = \sqrt{-1}$, μ_0 is the magnetic permeability of free space and ω angular frequency. For global (spherical) and local (Cartesian) problem setups, $\mathbf{r} = (r, \theta, \phi)$, and $\mathbf{r} = (x, y, z)$, respectively. Displacement currents are neglected in the considered period range, and the Fourier transform convention $e^{-i\omega t}$ is adopted. Note, that hereinafter the dependence of the fields on ω is omitted but implied.

Within an IE approach eqs (1)-(2) are reduced to the IE with respect to the electric field:

$$\mathbf{E}(\mathbf{r}) - \int_{V^1} \widehat{G}^{ej}_{1D}(\mathbf{r}, \mathbf{r}')\Delta\sigma(\mathbf{r}')\mathbf{E}(\mathbf{r}')dv' = \mathbf{E}_0(\mathbf{r}),\ \mathbf{r} \in V^1, \quad (3)$$

where V^1 is the region in which $\Delta\sigma = \sigma - \sigma_0 \neq 0$, σ_0 is the background 1-D conductivity distribution, $\mathbf{E}_0$ the background electric field, and $\widehat{G}^{ej}_{1D}$ the "electric" dyadic Green's tensor [*Kuvshinov and Semenov*, 2012; *Kruglyakov and Bloshanskaya*, 2017].

After solving eq. (3), the electric and magnetic fields at any location $\mathbf{r}$ are calculated as:

$$\mathbf{E}(\mathbf{r}) = \mathbf{E}_0(\mathbf{r}) + \int_{V^1} \widehat{G}^{ej}_{1D}(\mathbf{r}, \mathbf{r}')\Delta\sigma(\mathbf{r}')\mathbf{E}(\mathbf{r}')dv', \quad (4)$$

$$\mathbf{H}(\mathbf{r}) = \mathbf{H}_0(\mathbf{r}) + \int_{V^1} \widehat{G}^{hj}_{1D}(\mathbf{r}, \mathbf{r}')\Delta\sigma(\mathbf{r}')\mathbf{E}(\mathbf{r}')dv', \quad (5)$$

where $\mathbf{H}_0$ is the background magnetic field, and $\widehat{G}^{hj}_{1D}$ is the "magnetic" dyadic Green's tensor. Similarly as for the fields, the dependence of Green's tensors on ω is omitted but implied.

In the most of IE solvers, 1-D or 2-D fast Fourier transforms (FFT) are used to significantly decrease computational loads while performing the integration. For global simulations (invoking spherical geometry) the complexity is of order $O(N_\phi N_\theta^2 N_r^2)$, where

N_ϕ, N_θ and N_r are the number of cells in the ϕ-, θ- and r-directions, respectively. In local simulations (invoking Cartesian geometry) the complexity is of $O(N_x N_y N_z^2)$, where N_x, N_y and N_z are the number of cells in the x-, y- and z-directions. The usage of FFT requires a uniform grid in one (for global problem setups) or in two (for local problem setups) lateral directions. Due to the global nature of the sources which are responsible for GDS magnetic field variations, the OIE is generally modeled by means of global 3-D EM simulations. However, in order to simulate effects from small-scale bathymetry, global simulations based on a FFT-based IE approach require prohibitively high computational loads. The next section explains how this problem can be alleviated using a nested IE approach which couples global (spherical) and local (Cartesian) simulations.

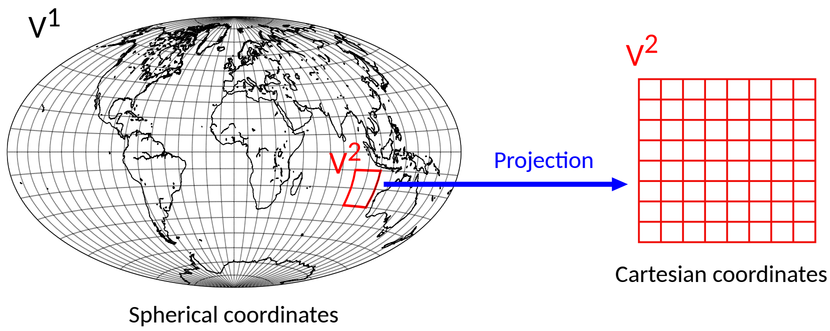

Figure 1. Setup for the global-to-Cartesian approach. V^1 is discretized by a coarse grid in spherical coordinates and V^2 is discretized by a fine grid in Cartesian coordinates.

2.2 Global-to-Cartesian (G2C) approach

The idea behind the approach is as follows. The whole (global) modeling domain, V^1, is divided into two parts: a local domain of interest, V^2, and its complement, V^1/V^2, as shown in Figure 1. Then eq. (3) can be rewritten as:

$$\mathbf{E}(\mathbf{r}) - \int_{V^2} \widehat{G}^{ej}_{1D}(\mathbf{r},\mathbf{r}')\Delta\sigma(\mathbf{r}')\mathbf{E}(\mathbf{r}')dv' = \mathbf{E}_0(\mathbf{r}) + \int_{V^1/V2} \widehat{G}^{ej}_{1D}(\mathbf{r},\mathbf{r}')\Delta\sigma(\mathbf{r}')\mathbf{E}(\mathbf{r}')dv', \ \mathbf{r} \in V^2. \quad (6)$$

This equation is a basis of the G2C approach. Specifically, V^1 is discretized by a coarse grid, and a global IE solver is utilized to compute "global" fields, $\mathbf{E}^{(g)}$ and $\mathbf{H}^{(g)}$, in V^1. In this paper we use the X3DG code to compute $\mathbf{E}^{(g)}$ and $\mathbf{H}^{(g)}$. Then, V^2 is discretized by a fine grid, and a Cartesian IE solver is exploited to compute "Cartesian" fields, $\mathbf{E}^{(C)}$

and $\mathbf{H}^{(C)}$ in V^2. In particular, eq. (6) for $\mathbf{E}^{(C)}$ reads:

$$\mathbf{E}^{(C)}(\mathbf{r}) - \int_{V^2} \widehat{G}_{1D}^{ej(C)}(\mathbf{r},\mathbf{r}')\Delta\sigma^{(C)}(\mathbf{r}')\mathbf{E}^{(C)}(\mathbf{r}')dv' = P_g^C \left[\mathbf{E}_0^{(g)}(\mathbf{r}) + \mathbf{E}^{add(g)}(\mathbf{r})\right], \ \mathbf{r} \in V^2. \quad (7)$$

After solving eq. (7), the electric field is calculated at any location $\mathbf{r} \in V^2$ as:

$$\mathbf{E}^{(C)}(\mathbf{r}) \ = \ P_g^C \left[\mathbf{E}_0^{(g)}(\mathbf{r}) + \mathbf{E}^{add(g)}(\mathbf{r})\right] + \int_{V^2} \widehat{G}_{1D}^{ej(C)}(\mathbf{r},\mathbf{r}')\Delta\sigma^{(C)}(\mathbf{r}')\mathbf{E}^{(C)}(\mathbf{r}')dv', \quad (8)$$

where

$$\mathbf{E}^{add(g)}(\mathbf{r}) = \int_{V^1/V^2} \widehat{G}_{1D}^{ej(g)}(\mathbf{r},\mathbf{r}')\Delta\sigma^{(g)}(\mathbf{r}')\mathbf{E}^{(g)}(\mathbf{r}')dv'. \quad (9)$$

The magnetic field at any location $\mathbf{r} \in V^2$ is calculated similarly. Here, the quantities with superscripts (g) and (C) denote those calculated using global and Cartesian IE solvers, respectively, and operator P_g^C projects the fields from a global (coarse) grid to a Cartesian (fine) grid. In our implementation of G2C approach the Mercator projection is exploited; for further details on this projection the reader is referred to *Snyder* [1982] and *Grayver et al.* [2019]. In this paper we use PGIEM2G code [*Kruglyakov and Kuvshinov*, 2018] to compute $\mathbf{E}^{(C)}$ and $\mathbf{H}^{(C)}$. The results of numerical tests aimed to verify the developed G2C approach are summarized in Supporting Information. It is relevant to note here that for simplicity of explanation we discuss above the two-step strategy, but the concept can be readily generalized to include multiple (nested) steps.

3 Results

Two geomagnetic observatories located at Cocos-Keeling (Intermagnet code of observatory: CKI) and Oahu (Intermagnet code: HON) islands, shown in Figure 2(b), are chosen to study the OIE in long-period responses.

3.1 Modeling island responses

We analyze magnetic field variations in the period range between a few days and a few months. There is a common consensus that these variations are due to a magnetospheric (ring current) source and are described via Y_1^0, the first zonal spherical harmonic in geomagnetic coordinates. Assuming this geometry one can determine the so-called local C-responses as [*Banks*, 1969]:

$$C_1(\mathbf{r}_a,\omega) = -\frac{a}{2}\tan\theta\frac{B_r(\mathbf{r}_a,\omega)}{B_\theta(\mathbf{r}_a,\omega)}, \quad (10)$$

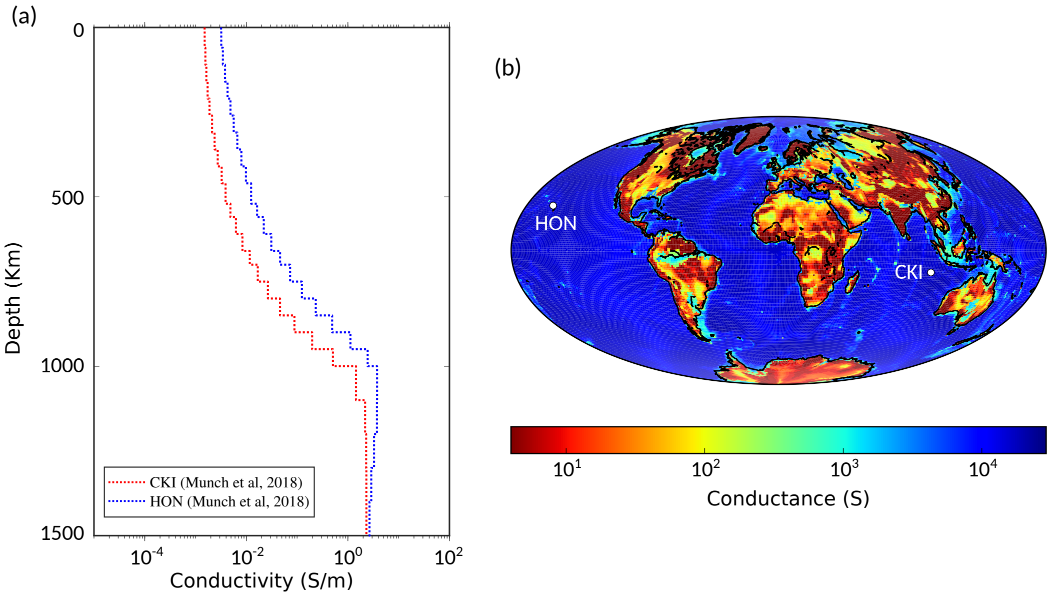

Figure 2. (a) 1-D conductivity profiles beneath CKI and HON observatories obtained by *Munch et al.* [2018], and (b) conductance of the surface thin shell used in global modeling and locations of CKI and HON observatories.

where a is the mean Earth's radius, and $\mathbf{r}_a = (a, \theta, \phi)$. To explore OIE in the responses we use a conductivity model which consists of a 1-D mantle overlaid by a surface thin shell of known laterally-variable conductance. For the periods considered in the paper – from 2.9 days to 83.2 days – the penetration depth varies approximately from 400 km to 1200 km, which is much larger than the depth of the oceans; thus, the surface thin shell of laterally-variable conductance is an adequate approximation of the nonuniform distributions of conductive oceans and resistive landmasses which are responsible for the OIE. To verify this, we calculated the responses in full 3-D models (not shown in the paper) and observed only negligible difference in the results. Global (shown in Figure 2b) and local (shown in Figure 3) conductance distributions are constructed using bathymetry data from the ETOPO1 Global Relief Model [*Amante and Eakins*, 2009], which has $0.016° \times 0.016°$ (arcmin) resolution. The land and seawater conductivities are set as $0.02\,\mathrm{S/m}$ and $3.2\,\mathrm{S/m}$, respectively; we ignore lateral variations of seawater conductivity, assuming that at considered periods the effects from such variations are small compared to those originating from conductivity contrasts between the ocean and land. In the course of G2C modeling a $8° \times 8°$ region is set as the local domain of fine grid simulations. We notice here that the lateral size of the local domain should be large enough to account for details of the bathymetry in the vicinity of observation site, but at the same time should be sufficiently small to minimize distortions from the projection. Actual size of the local domain ($8^\circ \times 8^\circ$) is justified by using the trial and error approach. The resolution of the conductance during the global modeling was fixed to $1^\circ \times 1^\circ$, whereas during G2C simulations we varied the cell sizes in the local domain which correspond to the conductance resolutions of $1^\circ \times 1^\circ$, $0.3^\circ \times 0.3^\circ$, $0.1^\circ \times 0.1^\circ$, $0.02^\circ \times 0.02^\circ$ and $0.01^\circ \times 0.01^\circ$.

As for 1-D mantle profile which underlay the surface shell, it varied during simulations depending on which observatory was considered. 1-D conductivity profiles beneath CKI and HON observatories (shown in Figure 2a) were obtained by *Munch et al.* [2018] through quasi 1-D inversion of the corresponding experimental local C-responses. Here the term "quasi" is used to stress the fact that during 1-D inversion the 3-D forward modeling operator was exploited by *Munch et al.* [2018] to account for OIE.

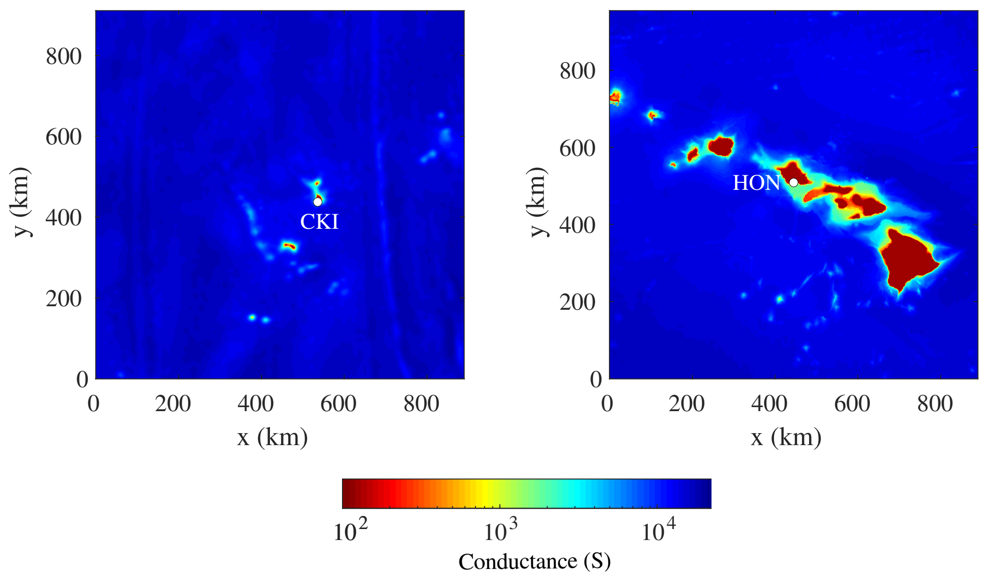

Figure 3. Local conductance distributions (of resolution $0.01^\circ \times 0.01^\circ$) in a vicinity of CKI and HON observatories.

Figure 4 presents real and imaginary parts of the modeled C-responses at CKI observatory. The responses calculated by global and G2C approaches using the same, $1^\circ \times 1^\circ$ resolution of conductance distribution, match well as expected. Small difference in the results at shorter periods is attributed to different numerical algorithms used in X3DG and PGIEM2G to solve the corresponding IE. Increase of resolution during G2C simulations from $1^\circ \times 1^\circ$ through $0.1^\circ \times 0.1^\circ$ to $0.02^\circ \times 0.02^\circ$ leads to significant changes

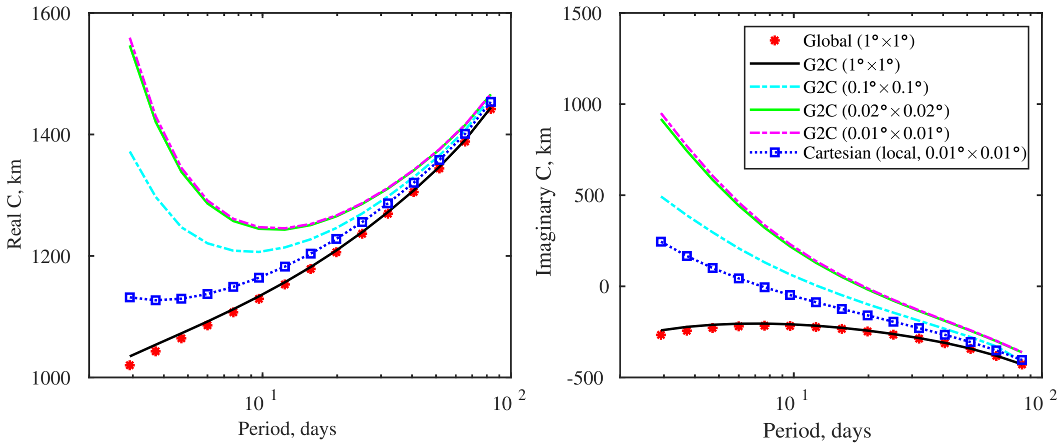

Figure 4. Modeled C-responses at CKI observatory. Responses are computed by X3DG using global conductance distribution of $1^\circ \times 1^\circ$ resolution, by the G2C approach using cell sizes in the local domain corresponding to conductance distributions of resolutions of $1^\circ \times 1^\circ$, $0.1^\circ \times 0.1^\circ$, $0.02^\circ \times 0.02^\circ$ and $0.01^\circ \times 0.01^\circ$, and by PGIEM2G only considering the local domain. 1-D profile from *Munch et al.* [2018] is used during the modeling.

in the responses, especially in the imaginary part, and overall at periods shorter than 20 days. Further increase of resolution up to $0.01^\circ \times 0.01^\circ$ change, however, the results rather insignificantly, in spite of the fact that $0.02^\circ \times 0.02^\circ$ and $0.01^\circ \times 0.01^\circ$ conductance distributions differ by construction. Two remarks are relevant at this point. First, the resolution as fine as $0.01^\circ \times 0.01^\circ$ is invoked in order to reproduce the actual distribution of conductance around this very small island which is only a few kilometers in size. Second, using finer than $0.01^\circ \times 0.01^\circ$ resolution during G2C modeling does not make sense since our conductance distributions are constructed using bathymetry model ETOPO1 which has a resolution of $0.016^\circ \times 0.016^\circ$. Summing up we can state that for this island the conductance distributions of $0.02^\circ \times 0.02^\circ$ or $0.01^\circ \times 0.01^\circ$ resolution have to be exploited in order to accurately account for the ocean induction effect.

However, for the relatively large islands, seemingly there is no need for such high-resolution modeling to account for the OIE in local C-responses, at least in the considered period range (from a few days to a few months). Figure 5 illustrates this fact. It presents the modeled C-responses at HON observatory. It is seen that the responses change insignificantly when the conductance resolution in the model is finer than $0.3^\circ \times 0.3^\circ$. We argue that for the HON observatory conductance distribution of $0.3^\circ \times 0.3^\circ$ resolution is sufficient to model OIE. Note, that other possible reason that different resolutions are needed for accurate modeling OIE at different islands is the distance between the observatory site and coast; for instance, CKI observatory is much closer to the coast than HON observatory.

One can ask is there a need to account for the distant structures (for instance, nonuniform distribution of oceans and continents) during local modeling, or in other words, whether the term $\mathbf{E}^{add(g)}$ in eq. (8) is indeed important? To address this question we set $\mathbf{E}^{add(g)}$ to zero and calculate C-responses (blue squares in Figures 4 and 5) using $0.01° \times 0.01°$ conductance resolution. It is seen that neglecting this term leads to rather different results. Thus, we conclude that both global and local structures must be taken into account.

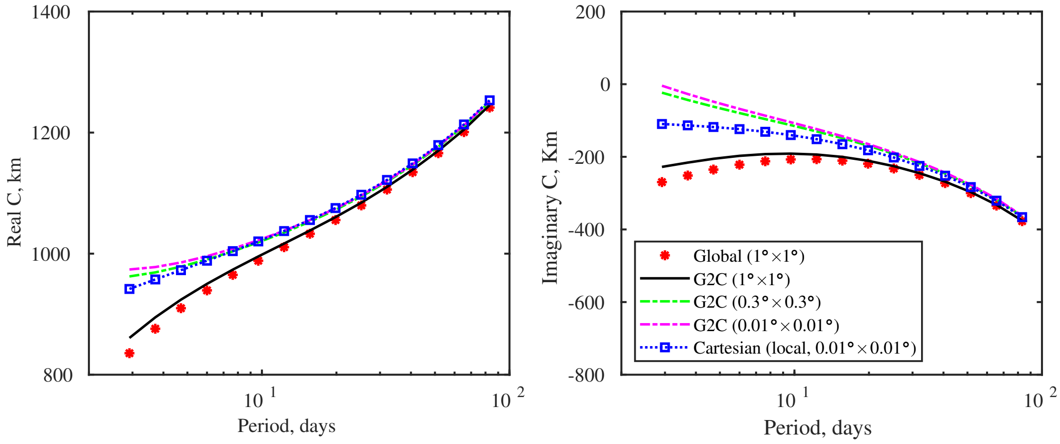

Figure 5. Modeled C-responses at HON observatory. Responses are computed by X3DG using global conductance distribution of $1° \times 1°$ resolution, by the G2C approach using cell sizes in the local domain corresponding to conductance distributions of resolutions of $1° \times 1°$, $0.3° \times 0.3°$, and $0.01° \times 0.01°$, and by PGIEM2G only considering the local domain. 1-D profile from *Munch et al.* [2018] is used during the modeling.

3.2 Obtaining new 1-D profiles beneath CKI and HON observatories

As it was discussed in Introduction, *Munch et al.* [2018] estimated long-period C-responses at a global net of geomagnetic observatories and performed their quasi 1-D inversion using the model which incorporated the surface shell with conductance distribution of $1° \times 1°$ resolution. They detected the pronounced disagreement between mod-

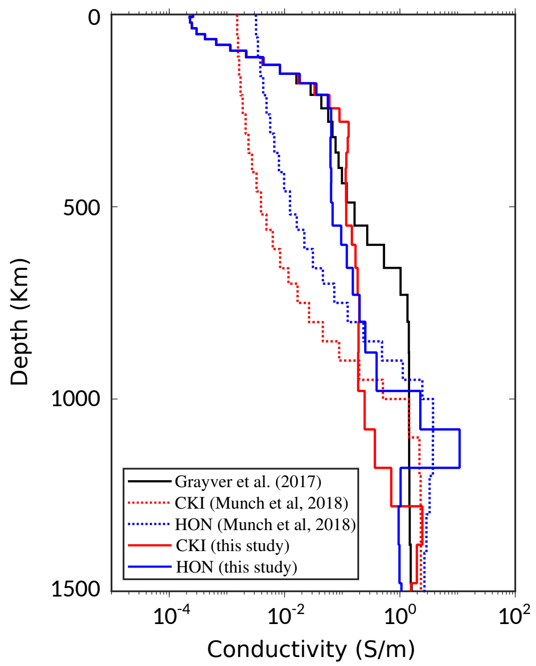

Figure 6. Obtained in this study (solid colored lines) and old (dashed colored lines) 1-D conductivity profiles beneath CKI and HON observatories. Black line depicts global 1-D profile from *Grayver et al.* [2017].

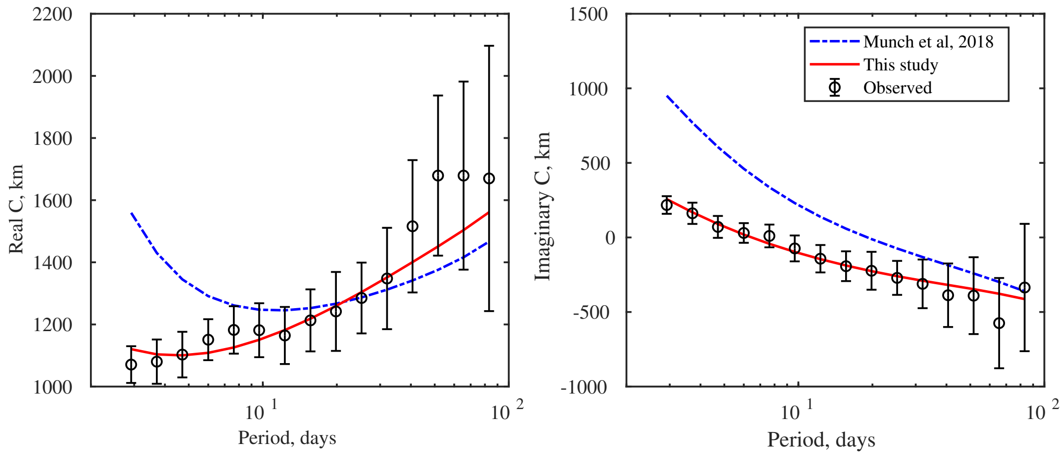

Figure 7. Modeled and observed C-responses at CKI observatory. The modeled responses are calculated by using 1-D profiles from *Munch et al.* [2018] and obtained in this study. Both modelings are performed by G2C approach with local conductance distribution of $0.01° \times 0.01°$ resolution. Observed responses are taken from *Munch et al.* [2018]. Uncertainties of the observed C-responses are indicated by the error bars.

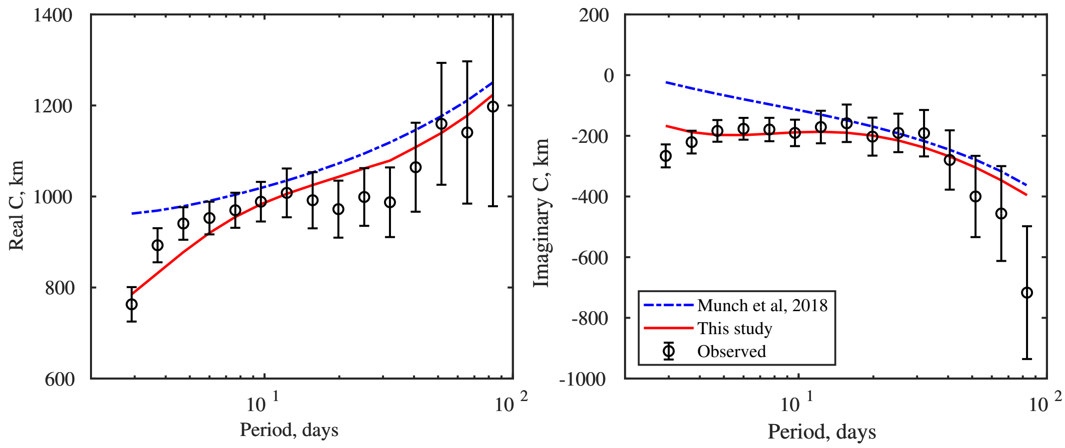

Figure 8. As in Figure 7, but for HON observatory.

eled and experimental C-responses at a number of island observatories, including CKI observatory. Moreover, *Munch et al.* [2018] observed anomalous behaviour of imaginary part of the experimental CKI responses, namely change of sign at shorter periods, which they failed to reproduce. Our model study described in previous section clearly demonstrate that this anomalous behavior is imitable if one uses during simulations the conductance distributions of finer resolution (cf. right plot in Figure 4). This result motivated us to invert C-responses obtained at CKI (and HON) observatories using "surface shell" models with as fine as practicable resolution of conductance distribution in a vicinity of observation sites. New 1-D conductivity models beneath these two islands were obtained as follows. We took 1-D profiles for CKI and HON obtained by *Munch et al.* [2018] and computed C-responses in the models with and without surface shell, denoted by $C^{\mathrm{1D+shell}}$ and C^{1D}, respectively. Computation of C-responses in the model with the surface shell was performed using G2C approach and exploiting local conductance distribution of $0.01^\circ \times 0.01^\circ$ resolution. Further we corrected the observed (i.e. estimated from the data) C-responses following the correction scheme of *Kuvshinov et al.* [2002]

$$C^{\mathrm{obs,corr}}(\mathbf{r}_a, \omega) = C^{\mathrm{obs}}(\mathbf{r}_a, \omega) \cdot \frac{C^{\mathrm{1D}}(\mathbf{r}_a, \omega)}{C^{\mathrm{1D+shell}}(\mathbf{r}_a, \omega)}. \tag{11}$$

Corrected responses were then inverted in terms of 1-D conductivity distribution. An inversion exploited Gauss-Newton optimization method as applied to a function consisting of the data misfit and regularization term. The regularization term in our implementation penalized the deviation of 1-D conductivity distribution from the reference 1-D model which was taken from *Grayver et al.* [2017]. Their model was obtained by joint inversion of satellite-detected tidal and magnetospheric signals and is believed to represent globally averaged 1-D mantle structure beneath the oceans. New and old 1-D profiles are shown in Figure 6 by dashed and solid colored lines, respectively. One can see that the new profiles are very different from those obtained by *Munch et al.* [2018]. At the same time they are very close to the reference model of *Grayver et al.* [2017] at depths 0 - 250 km which is not surprising since the responses at considered periods have very limited sensitivity to upper mantle structures. At depths 500 - 1200 km both profiles significantly differ from global 1-D profile of *Grayver et al.* [2017], moreover they noticeably differ between each other at depths 900 - 1200 km. It is interesting that the new 1-D profile beneath HON has a prominent enhancement in conductivity at depths 1000 - 1200 km.

Finally, C-responses were computed in the model with the $0.01° \times 0.01°$ surface shell and new 1-D mantle conductivity profiles underneath. Remarkably, modeled responses match very well (within the experimental uncertainties) with the observed responses for all considered periods and for both, real and imaginary, parts of the responses (cf. Figures 7 and 8). In particular we succeeded to quantitatively reproduce anomalous behavior (change of sign) of imaginary part of C-response at CKI observatory. In contrast, the modeled responses obtained in the model with the $0.01° \times 0.01°$ surface shell but with the old 1-D mantle conductivity profiles underneath differ much from the observed responses.

4 Conclusions

We revisit the ocean induction effect in long-period GDS responses at island observatories. A global-to-Cartesian (G2C) EM modeling methodology based on a nested IE approach is proposed to efficiently and accurately account for the effects from very local bathymetry. Two island, Cocos-Keeling and Honolulu, geomagnetic observatories, are chosen to study bathymetry effects in the local C-response. Numerical experiments demonstrate that very local bathymetry may dramatically influence the results, illustrating the importance of using high-resolution bathymetry when computing C-responses at island observatories.

By using G2C methodology, we obtain new 1-D conductivity models beneath considered islands and observe remarkable agreement between modeled and experimental responses. In particular, we succeeded to reproduce anomalous behavior of the responses at Cocos-Keeling observatory. An interpretation of the obtained models and their further adjustment including uncertainty quantification is beyond the scope of this paper, but will be the subject of future work. Furthermore, when combined long-period responses with global-to-local Sq transfer functions [*Guzavina et al.*, 2019] and magnetotelluric tippers [*Morschhauser et al.*, 2019], nested IE-based inversion would provide a unique opportunity for imaging the electrical structure of the oceanic mantle throughout its full depth range.

Acknowledgments

The authors acknowledge national institutes around the world that operate geomagnetic observatories, and INTERMAGNET (www.intermagnet.org) which promotes the high standards of observatory practice. We thank Federico Munch for providing us with the experimental responses and their uncertainties, as well as with 1-D conductivity profiles obtained in *Munch et al.* [2018]. We also thank William Lowrie for improving the English language of this paper. Moreover, we would like to thank two anonymous reviewers for their comments which significantly improve the manuscript. CC was supported by a grant from the China Scholarship Council Foundation (201806370223). MK and AK were partially supported by the European Space Agency through the Swarm DISC project. Bathymetry data used in this study are available at www.ngdc.noaa.gov/mgg/global/relief/ETOPO1/data/ice_surface/grid_registered/netcdf/.

References

Amante, C., and B. W. Eakins (2009), Etopo1 arc-minute global relief model: procedures, data sources and analysis, *Marine Geology and Geophysics Division*, *19*.

Banks, R. (1969), Geomagnetic variations and the electrical conductivity of the upper mantle, *Geophysical Journal International*, *17*(5), 457–487.

Buchen, J., H. Marquardt, S. Speziale, T. Kawazoe, T. B. Ballaran, and A. Kurnosov (2018), High-pressure single-crystal elasticity of wadsleyite and the seismic signature of water in the shallow transition zone, *Earth and Planetary Science Letters*, *498*, 77–87.

Fei, H., D. Yamazaki, M. Sakurai, N. Miyajima, H. Ohfuji, T. Katsura, and T. Yamamoto (2017), A nearly water-saturated mantle transition zone inferred from mineral viscosity, *Science Advances*, *3*(6), doi:10.1126/sciadv.1603024.

Grayver, A. V., F. D. Munch, A. V. Kuvshinov, A. Khan, T. J. Sabaka, and L. Tøffner-Clausen (2017), Joint inversion of satellite-detected tidal and magnetospheric signals constrains electrical conductivity and water content of the upper mantle and transition zone, *Geophysical Research Letters*, *44*(12), 6074–6081.

Grayver, A. V., M. van Driel, and A. V. Kuvshinov (2019), Three-dimensional magnetotelluric modeling in spherical Earth, *Geophysical Journal International*, *217*(1), 532–557.

Guzavina, M., A. Grayver, and A. Kuvshinov (2019), Probing upper mantle electrical conductivity with daily magnetic variations using global-to-local transfer functions, *Geophysical Journal International*, *219*(3), 2125–2147.

Karato, S.-i. (2011), Water distribution across the mantle transition zone and its implications for global material circulation, *Earth and Planetary Science Letters*, *301*(3-4), 413–423.

Karato, S.-i., and D. Wang (2013), Electrical conductivity of minerals and rocks, *Physics and Chemistry of the Deep Earth*, pp. 145–182.

Kelbert, A., A. Kuvshinov, J. Velímský, T. Koyama, J. Ribaudo, J. Sun, Z. Martinec, and C. J. Weiss (2014), Global 3-D electromagnetic forward modelling: A benchmark study, *Geophysical Journal International*, *197*(2), 785–814.

Khan, A. (2016), On earth's mantle constitution and structure from joint analysis of geophysical and laboratory-based data: An example, *Surveys in Geophysics*, *37*(1), 149–189.

Khan, A., A. Kuvshinov, and A. Semenov (2011), On the heterogeneous electrical conductivity structure of the earths mantle with implications for transition zone water content, *Journal of Geophysical Research: Solid Earth*, *116*(B01103), doi:10.1029/2010JB007458.

Kruglyakov, M., and L. Bloshanskaya (2017), High-performance parallel solver for integral equations of electromagnetics based on Galerkin method, *Mathematical Geosciences*, *49*(6), 751–776, doi:10.1007/s11004-017-9677-y.

Kruglyakov, M., and A. Kuvshinov (2018), Using high-order polynomial basis in 3-D EM forward modeling based on volume integral equation method, *Geophysical Journal International*, *213*(2), 1387–1401.

Kuvshinov, A. (2008), 3-D global induction in the oceans and solid earth: recent progress in modeling magnetic and electric fields from sources of magnetospheric, ionospheric and oceanic origin, *Surveys in Geophysics*, *29*(2), 139–186.

Kuvshinov, A., and A. Semenov (2012), Global 3-D imaging of mantle electrical conductivity based on inversion of observatory C-responses – I. An approach and its verification, *Geophysical Journal International*, *189*, 1335–1352.

Kuvshinov, A. V., N. Olsen, D. B. Avdeev, and O. V. Pankratov (2002), Electromagnetic induction in the oceans and the anomalous behaviour of coastal C-responses for periods up to 20 days, *Geophysical Research Letters*, *29*(12), 1–4, doi:10.1029/2001GL014409.

Morschhauser, A., A. Grayver, A. Kuvshinov, F. Samrock, and J. Matzka (2019), Tippers at island geomagnetic observatories constrain electrical conductivity of oceanic lithosphere and upper mantle, *Earth, Planets and Space*, *71*(1), 1–9, doi:10.1186/s40623-019-0991-0.

Munch, F. D., A. V. Grayver, A. Kuvshinov, and A. Khan (2018), Stochastic inversion of geomagnetic observatory data including rigorous treatment of the ocean induction effect with implications for transition zone water content and thermal structure, *Journal of Geophysical Research: Solid Earth*, *123*(1), 31–51.

Parkinson, W. D., and F. W. Jones (1979), The geomagnetic coast effect, *Rev. Geophys.*, *17*(8), 1999–2015, doi:10.1029/rg017i008p01999.

Schulze, K., H. Marquardt, T. Kawazoe, T. B. Ballaran, C. McCammon, M. Koch-Müller, A. Kurnosov, and K. Marquardt (2018), Seismically invisible water in earth's transition zone?, *Earth and Planetary Science Letters*, *498*, 9–16.

Snyder, J. (1982), Map projections used by the US Geological survey, *Tech. rep.*, US Government Printing Office.

Velímskỳ, J., A. Grayver, A. Kuvshinov, and L. Šachl (2018), On the modelling of m 2 tidal magnetic signatures: effects of physical approximations and numerical resolution, *Earth, Planets and Space*, *70*(1), 1–15, doi:10.1186/s40623-018-0967-5.

Yoshimura, R., and N. Oshiman (2002), Edge-based finite element approach to the simulation of geoelectromagnetic induction in a 3-D sphere, *Geophysical Research Letters*, *29*(3), 1–9, doi:10.1029/2001GL014121.

Yoshino, T. (2010), Laboratory electrical conductivity measurement of mantle minerals, *Surveys in Geophysics*, *31*(2), 163–206.

Yoshino, T., and T. Katsura (2013), Electrical conductivity of mantle minerals: role of water in conductivity anomalies, *Annual Review of Earth and Planetary Sciences*, *41*, 605–628.